Manuscript Number: ICARUS-14182R2

Title: Effects of radial motion on interchange injections at Saturn

Article Type: Regular Article

Keywords: Saturn; Magnetospheres; Saturn, magnetosphere

Corresponding Author: Dr. C. Paranicas,

Corresponding Author's Institution:

First Author: C. Paranicas

Order of Authors: C. Paranicas; Michelle F Thomsen; Nicholas Achilleos; Maria Andriopoulou; Sarah V Badman; George Hospodarsky; Caitriona M Jackman; Xianzhe Jia; Timothy Kennelly; Krishan Khurana; Peter Kollmann; Norbert Krupp; Philippe Louarn; Elias Roussos; Nick Sergis

Abstract: Charged particle injections are regularly observed in Saturn's inner magnetosphere by Cassini. They are attributed to an ongoing process of flux-tube interchange driven by the strong centrifugal force associated with Saturn's rapid rotation. Numerical simulations suggest that these interchange injections can be associated with inward flow channels, in which plasma confined to a narrow range of longitudes moves radially toward the planet, gaining energy, while ambient plasma in the adjacent regions moves more slowly outward. Most previous analyses of these events have neglected this radial motion and inferred properties of the events under the assumption that they appear instantaneously at the spacecraft's L-shell and thereafter drift azimuthally. This paper describes features of injections that can be related to their radial motion prior to observation. We use a combination of phase space density profiles and an updated version of a test-particle model to quantify properties of the injection. We are able to infer the longitudinal width of the injection, the radial travel time from its point of origin, and the starting L shell of the injection. We can also predict which energies can remain inside the channel during the radial transport. To highlight the effects of radial propagation at a finite speed, we focus on those interchange injections without extensive features of azimuthal dispersion. Injections that have traveled radially for one or more hours prior to observation would have been initiated at a different local time than that of the observation. Finally, we describe an injection where particles have drifted azimuthally into a flow channel prior to observation by Cassini.

We have made all the changes both referees have suggested.

Effects of radial motion on interchange injections at Saturn

C. Paranicas[1], M. F. Thomsen[2], N. Achilleos[3], M. Andriopoulou[4], S. V. Badman[5], G. Hospodarsky[6], C. M. Jackman[7], X. Jia[8], T. Kennelly[6], K. Khurana[9], P. Kollmann[1], N. Krupp[10], P. Louarn[11], E. Roussos[10], N. Sergis[12]

1. APL, 11100 Johns Hopkins Rd., Laurel, MD 20723
2. PSI
3. Univ. Coll. London, UK
4. SRI, Graz, Austria
5. Lancaster Univ., UK
6. Univ. of Iowa
7. Univ. of Southampton, UK
8. Univ. of Michigan
9. UCLA
10. MPI, Göttingen, Germany
11. IRAP, France
12. Academy of Athens, Greece

Additional contact information for above authors:

Corresponding author: chris.paranicas@jhuapl.edu, 1-240-228-8652
mthomsen@lanl.gov
nicholas.achilleos@ucl.ac.uk
maria.andriopoulou@oeaw.ac.at
s.badman@lancaster.ac.uk
hospodarsky@uiowa.edu
c.jackman@soton.ac.uk
xzjia@umich.edu
timothy-j-kennelly@uiowa.edu
kkhurana@igpp.ucla.edu
peter.kollmann@jhuapl.edu
krupp@mps.mpg.de
plouarn@irap.omp.eu
roussos@mps.mpg.de
nsergis@phys.uoa.gr

Icarus keywords: Saturn; Magnetospheres; Saturn, magnetosphere

Revision date: September 25, 2015

Abstract

Charged particle injections are regularly observed in Saturn's inner magnetosphere by Cassini. They are attributed to an ongoing process of flux-tube interchange driven by the strong centrifugal force associated with Saturn's rapid rotation. Numerical simulations suggest that these interchange injections can be associated with inward flow channels, in which plasma confined to a narrow range of longitudes moves radially toward the planet, gaining energy, while ambient plasma in the adjacent regions moves more slowly outward. Most previous analyses of these events have neglected this radial motion and inferred properties of the events under the assumption that they appear instantaneously at the spacecraft's L-shell and thereafter drift azimuthally. This paper describes features of injections that can be related to their radial motion prior to observation. We use a combination of phase space density profiles and an updated version of a test-particle model to quantify properties of the injection. We are able to infer the longitudinal width of the injection, the radial travel time from its point of origin, and the starting L shell of the injection. We can also predict which energies can remain inside the channel during the radial transport. To highlight the effects of radial propagation at a finite speed, we focus on those interchange injections without extensive features of azimuthal dispersion. Injections that have traveled radially for one or more hours prior to observation would have been initiated at a different local time than that of the observation. Finally, we describe an injection where particles have drifted azimuthally into a flow channel prior to observation by Cassini.

1. Introduction.

Injections of charged particles in Saturn's magnetosphere can be identified in multiple Cassini data sets. In terms of morphology, it is useful to separate interchange injections from more global injection processes. Interchange-related structures represent a means of transport that leaves the background magnetic field largely unperturbed, while global processes often involve large-scale magnetic reconfiguration. Based on their analysis of many events, Mitchell et al. (2014) found the former usually occur inward of about 12 R_S (1 Saturn radius = 60268 km), while the latter are more commonly observed outward of that distance. Interchange injections can be thought of as flux tube bundles (see, for instance, Burch et al. 2005) or flow channels (see below). A review of the literature on Saturn injections, including key findings, can be found in Thomsen et al. (2013).

Southwood and Kivelson (1987) and others have described conditions under which plasma distributions are unstable to the interchange process, which involve the radial gradient of both the entropy and the density or flux tube content. Since this work is focused on features of injected distributions that are measured by Cassini, we will not address the underlying physics of the instability.

In this work, we will focus on signatures of the radial motion of interchange injections as observed in the Cassini Plasma Spectrometer (CAPS) and Magnetosphere Imaging Instrument (MIMI) data sets (Young et al. 2004; Krimigis et al. 2004). Together these data sets cover the ion and electron thermal plasma and energetic charged particle energy ranges (eV to MeV). For brevity, we will use the term "injection" to mean "interchange injection" throughout this paper.

In plasma and charged particle data, injections can be observed, when the charged particle phase space density (PSD) profiles at constant adiabatic invariants varies as a function of radial distance from the planet. For example, an injection starting at high PSD and large L that moves inward into a region of lower PSD will appear as a flux enhancement since its initial PSD is approximately conserved (e.g., Mauk et al. 2005). Similarly, an injection initiated in a region of low PSD (as at low energies and larger radial distances) will appear as a depletion in the thermal plasma in the inner magnetosphere.

In addition to data analysis, we will also describe and employ a test particle model to make more quantitative the specific features that are a focus of this work. Our model significantly expands upon an earlier model we have used to study injections in charged particles above about 10 keV only (Paranicas et al. 2010). The chief modification of our model relates to the inclusion of a finite radial speed for the injection and the consequences for the trajectories of the test particles. These details are described fully below.

2. Injection model.

The picture of injections we employ is adopted from a simplified picture of the flow channels revealed by the Rice Convection Model (RCM) simulations of Liu et al. (2010). Specifically, we assume the creation of channels in which there is an inward plasma flow (i.e., a radial *E x B* drift motion of the particle guiding centers) with a constant value for a specified length of time, after which the inward velocity is zero. The model channel is taken to have a constant angular width in azimuth. We use a longitude system (SLS) based on Saturn kilometric radiation (SKR) modulation (see, Kurth et al. 2008, and references therein). For this model, the flow channel is always described in a corotating frame. It is important to keep in mind that this description is a better fit for some interchange injections than others. Other pictures such as flux tube bundles or even more elaborated fingers with merging and vortices (e.g., Hirake et al. 2012), probably fit other classes of observed injections better.

Assuming the test particle's motion can be approximated by the motion of its guiding center, we populate a grid in L shell and longitude with test particles. At each location we assume there is a range of energies at log-spaced intervals. In all, there are approximately one million test particles at the start of the simulation. We assume all particles begin to move inward from a narrow range of L shells around an L start (Ls) at constant inflow speed, conserving their first adiabatic invariant of motion in a dipolar magnetic field. In addition to this radial motion, we assume particles in the channel follow the same bulk corotation as the surrounding plasma and undergo energy- and species-dependent gradient-curvature drifts; both of these motions are in the azimuthal direction. Since the measured magnetic field strength inside injections is typically within a few percent of the surrounding field, we estimate these drifts using the background dipole of Saturn.

We compute the new characteristics of the test particles using a bounce-averaged, gradient-curvature drift approximation (Thomsen and Van Allen 1980). Halfway between the L steps, we update the test particle's energy and longitude. When the test particles reach the range of L shells of observation by Cassini (designated here as Lo), the simulation is stopped. Due to how our code is constructed, it is possible for observation L shells to be filled for up to 15 minutes leading to a small amount of azimuthal drift that can be observed in the simulations. Furthermore, this short filling time of the observation shells fits both pictures of the front of an injection channel and a flux tube bundle.

For the magnetic field orientation at Saturn, electrons have westward gradient-curvature drifts, while ions have eastward ones relative to the corotating channel. If they are not prohibited from drifting out of a flow channel, electrons can escape through the western edge and ions can escape through the eastern edge. Furthermore, the gradient-curvature drift speeds increase nearly linearly with particle energy. Burch et al. (2005) reasoned that the cross-section of a flux tube would lose particles as they drift out in this manner, the effect being more important at higher energies. They also inferred an inflow speed from this concept.

As described by Burch et al. (2005), another consequence of this drift-out effect is that the maximum energy that can be transported radially inward depends on the inflow speed. That is, for faster inflow speeds, energetic particles have less time to drift out of the flow channel during their radial transport. Thus faster inflow speeds mean higher energy particles can be delivered closer to the planet.

Figure 1 shows an example of an injection from the CAPS data set obtained on day 2005-104 at about 1500 UTC. For this time-energy spectrogram, the colors represent energy flux (energy times intensity). We propose this is an example of the drift out process that is the focus of this paper. The injection is widest below about 1 keV and narrows with increasing energy. During the plasma’s inward radial motion that is part of the interchange process, electrons drift away from the eastern edge of the flow channel towards then through the western edge (Burch et al. 2005). The effect is harder to see in cold to suprathermal plasma because that plasma travels around Saturn at nearly the local corotation speed. But at higher energies, the effect becomes very pronounced.

In creating simulated injections, we consider a narrow range of L shells (Lo) around the value corresponding to the *in situ* measurement. Near Lo, we keep track of test particles whether they are still inside the channel or whether they recently exited the channel. Cassini moves both radially and azimuthally across a flow channel when it encounters it and our model takes this into account.

The model we present here systematizes this drift-out process and provides an approach that can be exploited in the future for a much larger set of events in this class of injections to help understand the radial transport of interchange injections. It is important to note that we have carefully selected events for this study that show features we believe are due to the drift out process. Many interchange events do not show such characteristics.

3. Influence of starting L shell and inward flow speed.

In this section, we show some results of the test particle model to describe the kinds of effects we anticipate and their causes. For the cases we describe in this section, we will use the same spacecraft ephemeris information for an actual injection, that we will analyze in the next section, observed on day 2007-321 at about 01:10 UTC by both CAPS/ELS and MIMI/LEMMS. ELS is the Electron Spectrometer and LEMMS is the Low Energy Magnetosphere Measurement System sensor. At the time of this observation, the spacecraft was at about Lo=5.9 and at a few degrees north latitude in the magnetosphere. In each simulation, we launch approximately one million test particles from a region around Ls; the exact number depends on how well the results cover the final energy range. Around Lo, we find the eastern and western edges of the injected population at a set of representative energies. Below we refer to the “leading” edge of the injected test particles as the edge that is first encountered by Cassini (i.e., the left hand edge of the particles in the time-energy spectrograms we use here) and the “trailing” edge as the boundary of the test particle population that is detected last.

In Figures 2 and 3, we assume the test particles are electrons initially populating 2.65^o of Saturn longitude. In Figure 2, we assume the radial speed of the test particles is 20 km/s and we vary Ls to produce the displayed curves. There are three start locations: Ls=7.2 (solid black curve), Ls=8.0 (solid gray curve), and L=11.0 (dotted black curve). The total radial drift time between the start and stop L shells can be found from, td = (Ls - Lo)/vr. The injection described by the solid black line has the shortest total radial transport time and therefore this channel contains the highest energies among the three cases. The highest energy particles did not have sufficient time to drift azimuthally out of the channel because of the short radial drift time and the large azimuthal width. It is also worth noting in Figure 2, near the lowest energies of the curves (around 1 keV), the particles that crossed the largest range of L shells gained the most energy.

In Figure 3, we simulate the same channel as in Figure 2, but this time we vary the radial speed, keeping Ls = 8.0 in all cases. The inflow speeds are vr=35 km/s (black solid curve), 20 km/s (gray curve), and 10 km/s (black dotted curve). Again, for the most rapid radial transport (or equivalently the shortest total radial drift time), energetic electrons do not have as much time to drift azimuthally out of the channel before reaching Lo. Therefore the highest energy injection at Lo corresponds to the most rapid inflow speed when all the injections start at the same Ls.

We also note that the way our model works, the observation L shell is filled for slightly different amounts of time depending on the radial inflow speed. The dotted black line corresponds to filling for about 15 minutes (in the other 2 cases, these L shells are filled for a shorter amount of time). This does not change the maximum energy, but shifts the point (where the leading and trailing edges meet) slightly to the right in the figure. The longer Lo is filled, the more azimuthal drift on the shell we expect. We plan to take up the features associated with azimuthal drift on the observation L shell more extensively in a later study.

Figures 2 and 3 show that both Ls and vr affect the upper cutoff energy of the injected distribution. However, the fundamental dependence is actually the total radial transport time, which is a combination of the two. When the simulations are run varying both Ls and vr such that the radial drift time is constant, the variation of the cutoff energy is much less than when either Ls or vr is varied alone. Indeed, if it weren't for the L-dependence of the azimuthal drift speed, the profiles with the same td would be identical. These idealized cases show that if Ls can be estimated, the upper energy cutoff of the observed signature can be used to constrain the inflow speed.

4. Data-model comparisons.

As noted above, the total inward travel time governs the final shape of the injection, and Ls and vr cannot be separately determined from a given injection profile. Therefore, we attempt to narrow parameter space by using the phase space density profile of the particles and the assumption that during the relatively rapid radial transport, the phase space densities are conserved for constant adiabatic invariants. Rymer et al. (2009) used the PSD along the orbit during which the injection was observed to infer a starting location of the injection in their analysis. Here we will use both the recent PSD profile (i.e., from orbital data obtained around the time the injection was observed) and also the mission-averaged PSD profile to estimate Ls.

In Figure 4, we show two PSD profiles corresponding to electrons with 2 keV at the observation location. Both profiles average over all pitch angles and assume adiabatic heating of particles with 70^o equatorial pitch angles, similar to the model assumptions. The black line shows computed PSD from data obtained around the beginning of day 2007-321 and throughout the inbound part of the Cassini orbit. The injection is clearly visible as the peak in PSD around L=5.9 (vertical dotted line). The orange line is a mission-averaged PSD profile corresponding to the same values of the invariants. To estimate Ls from these data, we use the mission-averaged profile, which has a more monotonic character. We adopt Ls=7.2 as the “point of origin” of this injection because the PSD at this L shell is the same as the event at Lo~5.9 (vertical green line). Figure 5 shows LEMMS electron intensity plots from the same time period. Based on the MIMI data (which was sampling nearly field-aligned particles at this time), we would estimate the upper energy cutoff of the injection to be 60 keV. To achieve this upper energy with Ls=7.2 requires vr ~18 km/s in our simulation, corresponding to a radial transport time of about 1.2 hours.

In Figure 6, we show a spectrogram of ELS and LEMMS data from this time period and two sets of modeled edges. The ELS data have a constant background value subtracted so that the transition near 20 keV between ELS and LEMMS is smoother in intensity. The leading and trailing edges at the higher energies that overlay the data correspond to vr~18 km/s, as discussed above. We also included a fit at 9 km/s (set of leading and trailing edges at lower energy) since the ELS and LEMMS data correspond to different local pitch angles, leading to some uncertainty in the fitting process. At equal energy, field-aligned particles gradient-curvature drift slower than equatorially-mirroring ones. Therefore it is possible in this case that the more field-aligned MIMI data show a slightly higher maximum energy than if it were measuring the same pitch angles as ELS. Finally, these spectrograms provide a good picture of the injection and the surrounding plasma, but near the transition in energy between the two instruments, it is harder to make out subtle changes in intensity. We have found that line plots (such as in Figure 5) are more useful in identifying the peak energy needed in the model to constrain the inflow speed.

In Figure 7, we show another time-energy spectrogram using only ELS data obtained on day 2005-068 beginning at 02:00 UTC. As in all the injections we show in this paper, the spacecraft was close to the magnetic equator when the injection was detected. For the data shown, ELS was measuring electrons with approximately 90^o local pitch angle. We simulated this injection assuming electrons with a mirror latitude of 5^o and superimposed the leading and trailing edges from our model on the data. Next we describe how the model parameters were chosen for this fit.

The PSD profile in Figure 8, corresponding to 600 eV electrons in the observed injection, shows an analysis for this event that is similar to that shown in Figure 4. To model this event, we assume Ls=8.55. In Figure 9, we show line plots of the three lowest energy LEMMS electron channels from this time period. A remnant of the injection is visible in channel C0 (just prior to 02:19 UTC), but it does not seem to appear at higher energies. This guides our choice of the upper energy cutoff to be ~ 27 keV. From these considerations, for the fit displayed in Figure 6, we use a longitudinal width of 1.7°, initial energies of 125 eV to 1 MeV, and vr=18.2 km/s, corresponding to a total radial drift time of td~1.3 hours, with the results shown in Figure 7.

5. Evidence for drift into the channel.

In this section, we discuss how features associated with the radial motion of the particles can be used to analyze more complex injections. In Figure 10, we show two closely related injections observed by ELS and LEMMS on day 2006-080 at Lo of 7.3-7.4. Previously some analysis has been carried out on these injections in the MIMI energy range (Paranicas et al. 2008; Mitchell et al. 2015). Paranicas et al. (2008) suggested that if these separate injections are isolated flux tubes, it is then hard to reconcile the data at high energy. This is because at some pitch angles, the older bands of dispersing particles, visible above about 100 keV in the MIMI data, are the same inside and outside the events. Mitchell et al. (2015) expanded on the analysis of this time period showing mostly MIMI ion data and pitch angle dependence. They presented magnetometer data indicating an increase in Bz of 11-12% inside the injection compared to the surrounding plasma.

The two injections shown in Figure 10 are roughly confined to these time boundaries: 04:24 – 04:35 UTC and 04:45 – 04:54 UTC. The horizontal stripe between about 20 and 40 keV (note that the y axis shows the logarithm of energy) is an instrument artifact caused by sunlight entering the LEMMS telescope. Below this energy, the electron population looks similar to what we have discussed in the previous sections, exhibiting drift-dispersion and leakage out of the channel on the trailing side (see the faint distribution, for instance, extending to the right from about 04:54 UTC in the tens of keV energies). Because of the light contamination, this injection was not ideal to model. However, we carried out a coarse fit to the electrons observed between about 04:27 and 04:35 UTC, assuming this group of electrons has a cutoff energy of 35 keV. Other parameters used to fit the data were: 3.7^o longitudinal width, electron energies of 1 keV to 1 MeV at Ls=9.0 (determined by the PSD matching technique), and vr~14 km/s (necessary to produce a maximum energy of 35 keV); this corresponds to, td~2.15 hours.

The presence of enhanced fluxes of electrons at energies well above the apparent cutoff we have modeled, with strict confinement to the same longitudes as the suprathermal particles, is a more peculiar aspect of these data. The issue is that between 04:44 and 04:54 UTC, for instance, at energies above 10 keV, the spacecraft encounters a flux enhancement at all energies at the same time. But these particles drift at different rates around the magnetosphere. So the question is why are they not dispersed.

We propose the following interpretation of these data. When a flow channel forms or “opens” and creates a radial pathway between L shells, particles drift inward. As we have described in this paper, during this inward radial drift, some electrons will drift sideways out of the channels, depending on parameters such as their energy and their longitude with respect to the channel edges. However, it is also possible for ambient electrons to drift into the channel at all positions along its radial path. As this occurs, they experience the increased magnetic field strength within the channel and gain perpendicular energy, due to the conservation of the first adiabatic invariant of motion. Furthermore, energetic charged particles entering the channel in this manner also gain energy as they drift radially inward toward the planet. Both of these effects lead to a flux enhancement inside the channel compared to the surroundings. Since these particles enter the channel at different radial distances and are in different stages of drifting across the channel, they can fill the channel in a more uniform way. That is, they do not have the coherent drift out signatures seen in the main population of the injection at lower energies.

Considering a flux tube picture, Mitchell et al. (2015) also required non-equatorial particles around 100 keV (for the same day 2006-080 event) to drift into the flux tube. We are viewing the 2006-080 data in the context of a radially extended flow channel. In such a picture, particles from the surroundings continuously drift into the channel and are carried radially inward by it. This is a useful picture for some events because the channel structure itself provides a means by which energetic charged particles can be further energized and carried radially inward toward Saturn. When the channel eventually closes or the inward flow is halted, it is possible that these populated structures disperse and create the bands that are seen in the MIMI data (Paranicas et al. 2011). Such bands can extend over several L shells.

6. Discussion.

The test particle model described above helps us to understand features in interchange injections observed by Cassini. In particular, we have illustrated that because of the drift-out effect at finite inflow speeds, an upper cutoff energy exists in the injected population, which can tell us about the radial drift time of the injection. For the three events we modeled in detail here, we found radial drift times of ~1.2-2.4 hrs, 1.3 hr, and 2.2 hr. This radial travel time must be included in a determination of the local time of origin of these events and would shift the inferred local time of the injection origin. Previous analyses of the distribution of local times of injections [e.g., Chen and Hill 2008; Kennelly et al., 2013] have neglected this radial transport time and would therefore not accurately reflect the actual local time of origin.

The radial flow speeds we have estimated for these three events (~9 to 18 km/s) are reasonably consistent with the few previous estimates of inflow speed (e.g., Burch et al., 2005; Rymer et al., 2009; Chen et al., 2010). This analysis should be expanded to a larger population of events to establish the range of variability and the radial dependence of the inflow speed.

In this study, we have focused on the effects that are related to the inward radial transport of the individual particles. For simplicity, we have assumed in our model that the electromagnetic fields in the flow channel mirror those in the surrounding medium, except for the electric field that drives the radial motion. A feature we have ignored here is the magnetic gradient at the azimuthal edges of the flow channel (see, for example, Mitchell et al. 2015). This gradient will likely cause an additional radial drift along the flow channel edges as particles drift azimuthally toward the edges. Put another way, as particles reach the edges and begin to exit the channel, they may have components of azimuthal and radial drift. This may explain why regions just external to the channel are often not coherently populated by particles that exited the channel onto that L shell earlier (i.e., during the time the channel was open at that L shell prior to observation).

The use of the PSD profile in constraining Ls also contains uncertainties. For each value of the first adiabatic invariant in the measured injection, both the recent and the average profile can vary. We have attempted to survey parameter space by looking at Ls for various energies and pitch angles, but a more systematic approach would be desirable.

A main conclusion of this paper is that we expect charged particles to drift azimuthally in and out of flow channels during their inward motion. That is, the flow channel boundaries, in the limited cases we have surveyed, do not prohibit this motion. A consequence of this conclusion relates to how the channel structure limits the energies of particles that can be carried inward. Channels that are very narrow in azimuthal width cannot transport energetic particles as deeply into the inner magnetosphere as wider channels can, if other parameters are the same. Also, we have shown that unless the inflow speed is large, energetic particles drift sideways out of the channel and there is a limit to how efficiently the radiation belts can be supplied with high energy particles within the context of flow channels.

Acknowledgements. The authors would like to thank CAPS and MIMI for use of their data. We would like to acknowledge ISSI-Bern for hosting our research team and making this paper possible. CP appreciates CDAPS and other grants between NASA and JHU that supported his efforts. He would also like to thank D. G. Mitchell for useful conversations about magnetic gradients near injection edges. Work at PSI was funded by the NASA Cassini program through JPL contract 1243218 with SWRI. In the US, the Cassini project is managed by JPL for NASA. MFT is grateful to LANL for the support provided to her as a guest scientist. CMJ was supported by a Science and Technology Facilities Council Ernest Rutherford Fellowship.

References.

Burch, J. L., et al. (2005), Properties of local plasma injections in Saturn's magnetosphere, *Geophys. Res. Lett., 32*, L14SO2.

Chen, Y., T. W. Hill, A. M. Rymer, and R. J. Wilson (2010), Rate of radial transport of plasma in Saturn's inner magnetosphere, *J. Geophys. Res., 115,* A10211.

Chen, Y., and T. W. Hill (2008), Statistical analysis of injection/dispersion events in Saturn's inner magnetosphere, *J. Geophys. Res.*, *113*, A07215.

Hirake, Y., F. Tsuchiya, and Y. Katoh (2012), Io torus plasma transport under interchange instability and flow shears, *Planet. Space Sci., 62,* 41.

Krimigis, S. M. (2004), Magnetosphere imaging instrument (MIMI) on the Cassini mission to Saturn/Titan, *Space Sci. Rev.*, *114*, 233-329.

Kurth, W. S., T. F. Averkamp, D. A. Gurnett, J. B. Groene, and A. Lecacheux (2008), An update to a Saturnian longitude system based on kilometric radio emissions, *J. Geophys. Res., 113,* A05222.

Liu, X., et al. (200), Numerical simulation of plasma transport in Saturn's inner magnetosphere using the Rice Convection Model, *J. Geophys. Res., 115,* A12254.

Mauk, B. H., et al. (2005), Energetic particle injections in Saturn's magnetosphere, *Geophys. Res. Lett.*, *32*, L14S05, doi:10.1029/2005GL022485.

Mitchell, D. G., et al. (2015), Injection, interchange, and reconnection: Energetic particle observations in Saturn's magnetosphere, in *Magnetotails in the Solar System*, A. Keiling, C. M. Jackman, and P. A. Delamere, (Eds.), pp. 327-344, AGU Geophysical Monograph 207, John Wiley & Sons.

Paranicas, C., et al. (2010), Transport of energetic electrons into Saturn's inner magnetosphere, *J. Geophys. Res., 115,* A09214, doi:10.1029/2010JA015853.

Paranicas, C., et al. (2008), Energetic charged particle injections at Saturn, AGU, Fall Meeting, 2008AGUFMSM32A.03P

Rymer, A., et al. (2009), Cassini evidence for rapid interchange transport at Saturn, *Planet. Space Sci.*, *57*, 1779-1784.

Southwood, D. J., and M. G. Kivelson (1987), Magnetospheric interchange instability, *J. Geophys. Res.*, *92*, 109.

Thomsen, M. F. (2013), Saturn's magnetospheric dynamics, *Geophys. Res. Lett.*, *40*, 5337-5344, 2013GL057967.

Thomsen, M., and J. A. Van Allen (1980), Motion of trapped electrons and protons in Saturn's inner magnetosphere, *J. Geophys. Res.*, *85*, 5831-5834.

Young, D. T., et al. (2004), Cassini plasma spectrometer investigation, *Space Sci. Rev.*, *114*, 1-112.

Figure captions.

Figure 1. Time-energy spectrogram of CAPS ELS data obtained on day 2005-104. Energy flux during this event is most intense at the highest energies displayed on the right-hand side. This paper suggests this feature is due to the gradient-curvature drift of energetic electrons causing losses through the western edge (right-hand edge in this display) of a flow channel.

Figure 2. Leading (left-hand side) and trailing (right-hand-side) edges for a series of test particles launched from different L starts with a common radial drift speed of 20 km/s. The edges correspond to test particles that can be detected by Cassini, using its ephemeris information on day 2007-321. Test particles have energies between 200 eV and 1 MeV at Ls and mirror latitudes of 10^o.

Figure 3. Same display type as Figure 2. Here we keep Ls=8.0 and vary the radial speed. The black solid curve corresponds to vr=35 km/s, the solid gray curve is vr=20 km/s, and the dotted black curve is vr=10 km/s.

Figure 4. Electron phase space density as a function of dipole L shell for recent time (black curve) and mission-averaged data (orange curve). Data are averaged over all pitch angles to improve statistics. The PSD calculation is based on 70^o equatorial pitch angles. A vertical dotted blue line shows the injection in question.

Figure 5. Line plots of the intensity of tens of keV electrons detected by LEMMS around the time of the injection on day 2007-321. The figure shows six separate energy channels. During this time, the spacecraft is at a few degrees north latitude.

Figure 6. Overlay of ELS and LEMMS time-energy spectrogram and two sets of modeled injection edges. The injection had a longitudinal width of 2.65^o. At Ls=7.2, the electrons had energies between 200 eV and 1 MeV, with a mirror latitude of 10^o. The mirror latitude is chosen to correspond to the equatorial pitch angle detected by ELS during the observation.

Figure 7. Time-energy spectrogram of ELS data obtained on day 2005-068. We model the second injection feature and superimpose an outline created from the test particles in the simulation.

Figure 8. Electron PSD as a function of dipole L shell for recent time (black curve) and mission-averaged data (orange curve). The PSD calculation is based on 80^o equatorial pitch angles. A vertical dotted line shows the same injection that is described in Figures 7 and 9.

Figure 9. Line plots of the intensity of tens of keV electrons detected by LEMMS around the time of the injection. The maximum energy of the injection is detected in the lowest energy electron channel of LEMMS.

Figure 10. Two closely related injections observed by Cassini on day 2006-080. The time-energy spectrogram shows a limited energy range near the transition energy between ELS and LEMMS. The y-axis is in log10 (E in keV). The horizontal stripe at energies just above 20 keV is due to light contamination in the LEMMS sensor.

Figure 1

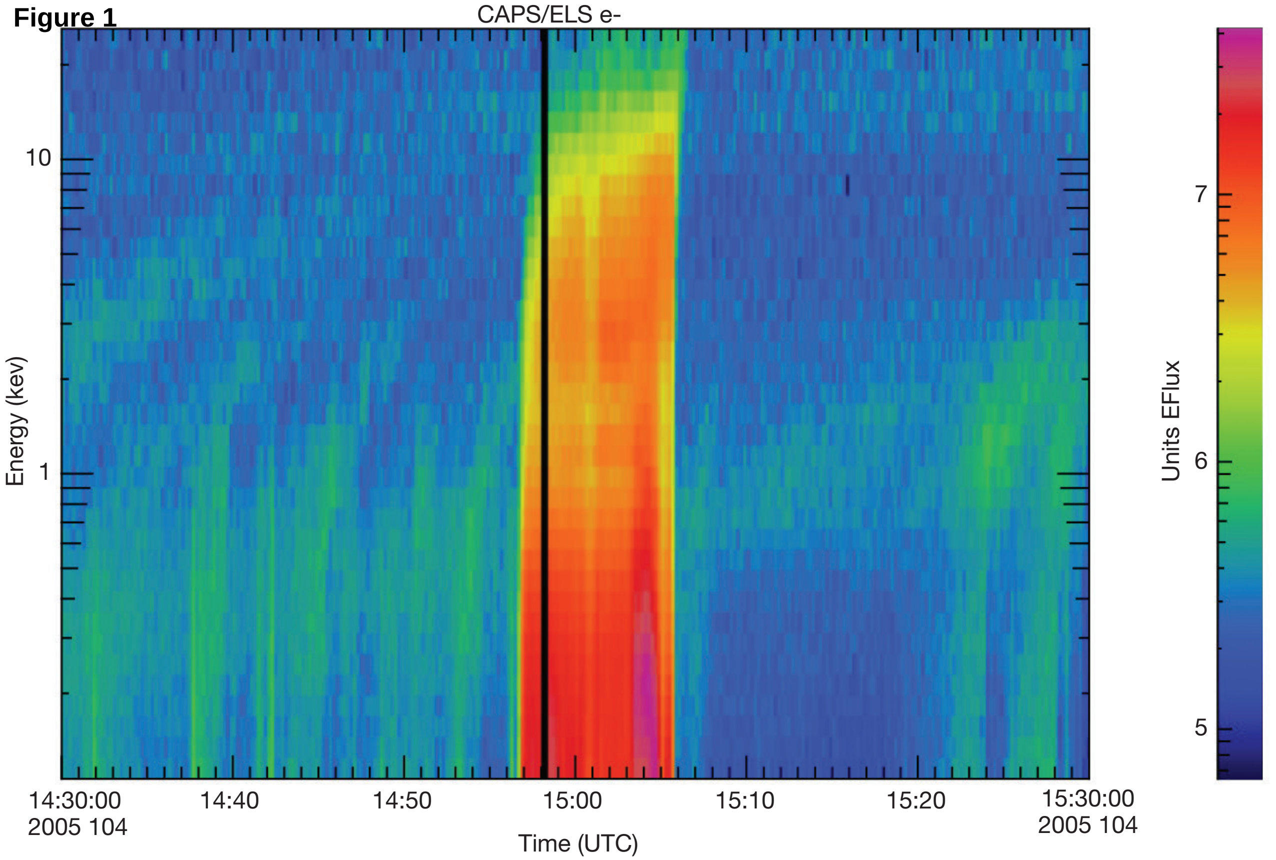
CAPS/ELS e-
Energy (kev)
10
1
14:30:00
2005 104
14:40
14:50
15:00
15:10
15:20
15:30:00
2005 104
Time (UTC)
Units EFlux
7
6
5

Figure 2

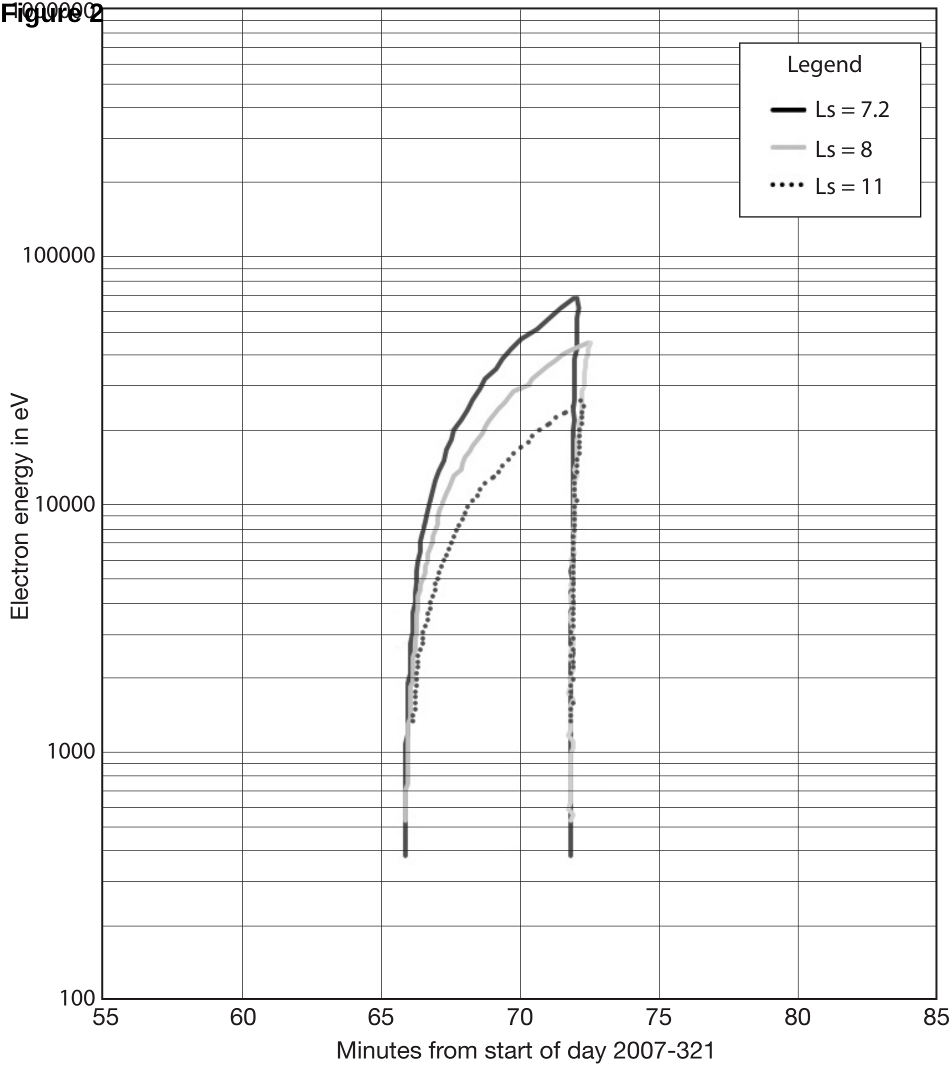
1000000
100000
10000
1000
100
Electron energy in eV
55
60
65
70
75
80
85
Minutes from start of day 2007-321
Legend
Ls = 7.2
Ls = 8
Ls = 11

Figure 3

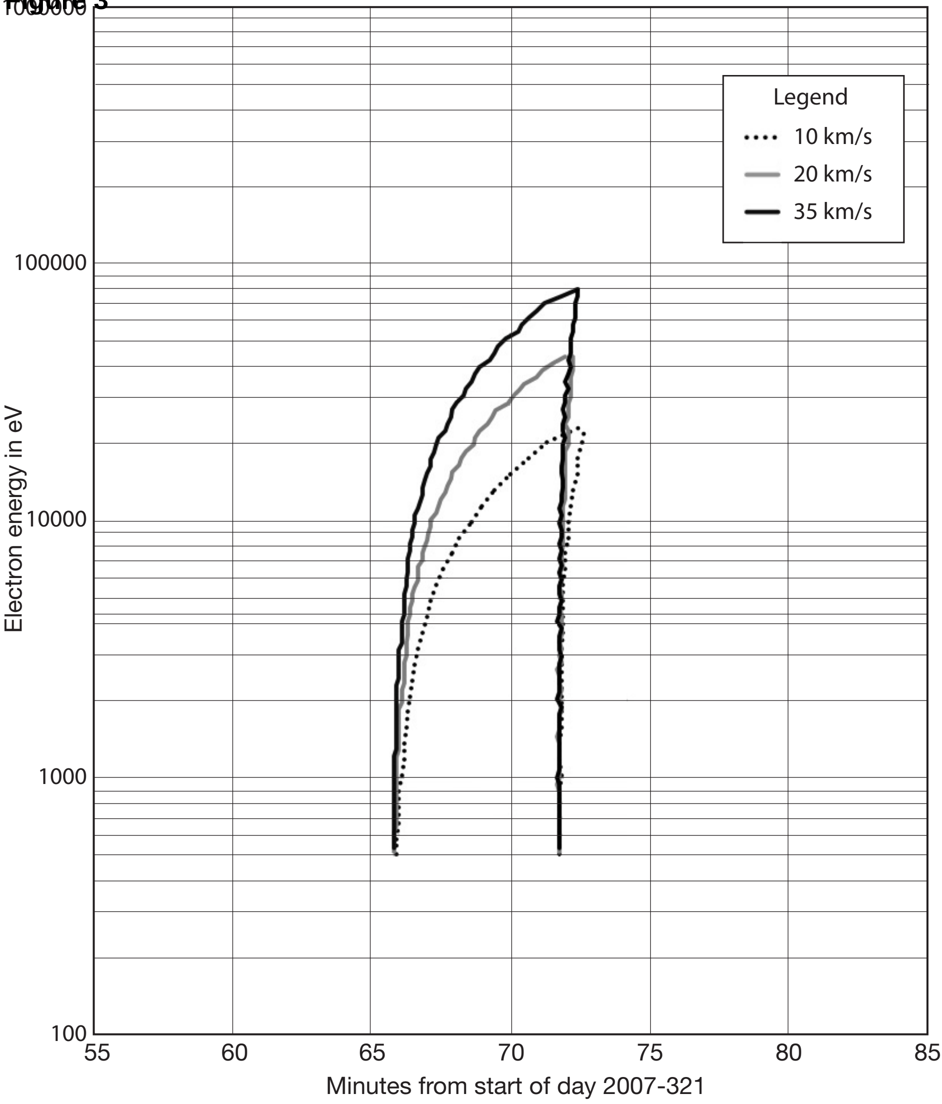
1000000
100000
10000
1000
100
Electron energy in eV
55
60
65
70
75
80
85
Minutes from start of day 2007-321
Legend
10 km/s
20 km/s
35 km/s

Figure 4

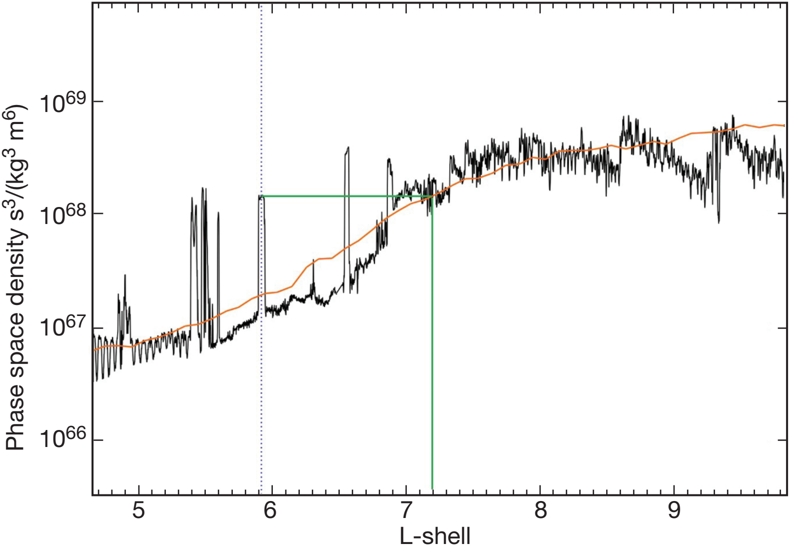

Phase space density s^3/(kg^3 m^6)
10^69
10^68
10^67
10^66
5
6
7
8
9
L-shell

Figure 5

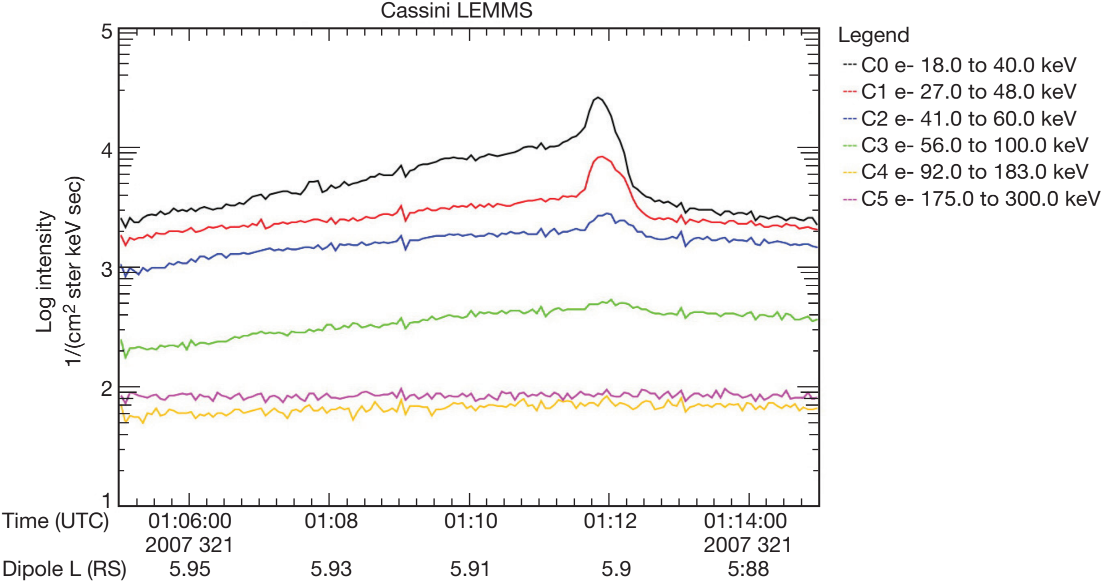
Cassini LEMMS
Log intensity
1/(cm2 ster keV sec)
5
4
3
2
1
Legend
C0 e- 18.0 to 40.0 keV
C1 e- 27.0 to 48.0 keV
C2 e- 41.0 to 60.0 keV
C3 e- 56.0 to 100.0 keV
C4 e- 92.0 to 183.0 keV
C5 e- 175.0 to 300.0 keV
Time (UTC)
01:06:00
2007 321
01:08
01:10
01:12
01:14:00
2007 321
Dipole L (RS)
5.95
5.93
5.91
5.9
5:88

Figure 6

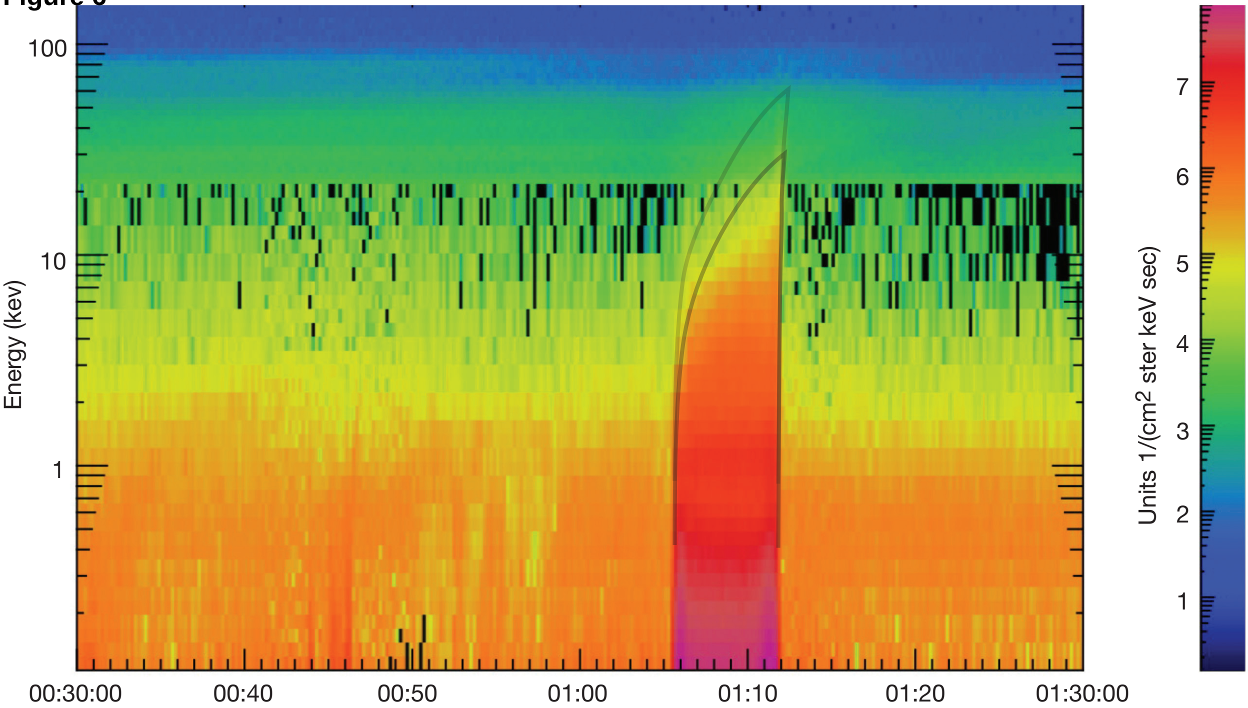
100
10
1
Energy (kev)
00:30:00
00:40
00:50
01:00
01:10
01:20
01:30:00
Units 1/(cm2 ster keV sec)
7
6
5
4
3
2
1

Figure 7

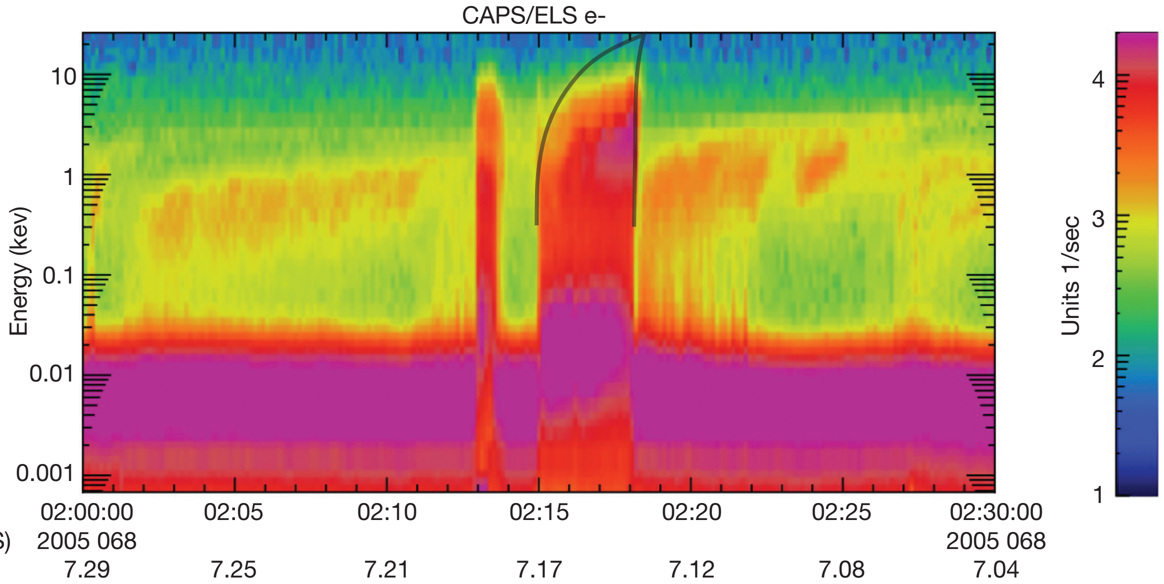
CAPS/ELS e-
Energy (kev)
10
1
0.1
0.01
0.001
Units 1/sec
4
3
2
1
Time (UTC)
Dipole L (RS)
02:00:00
2005 068
7.29
02:05
7.25
02:10
7.21
02:15
7.17
02:20
7.12
02:25
7.08
02:30:00
2005 068
7.04

Figure 8

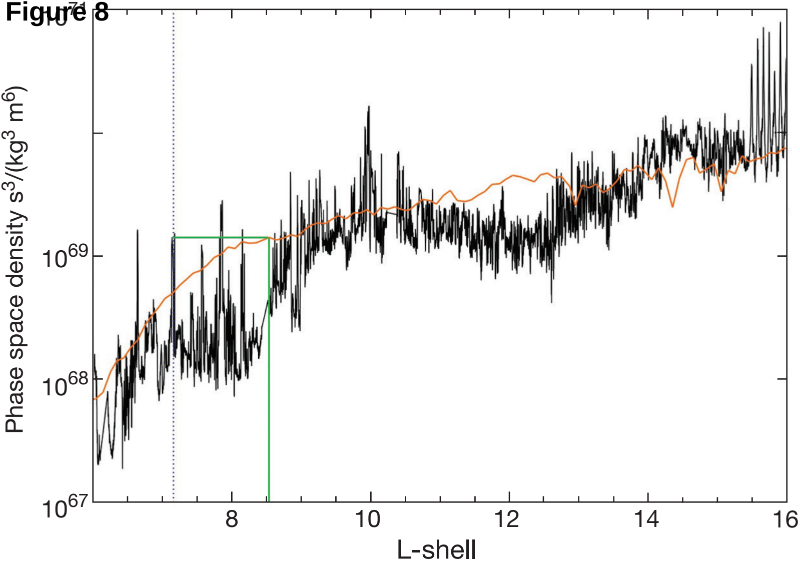
10^{71}
10^{69}
10^{68}
10^{67}
Phase space density s^3/(kg^3 m^6)
8
10
12
14
16
L-shell

Figure 9

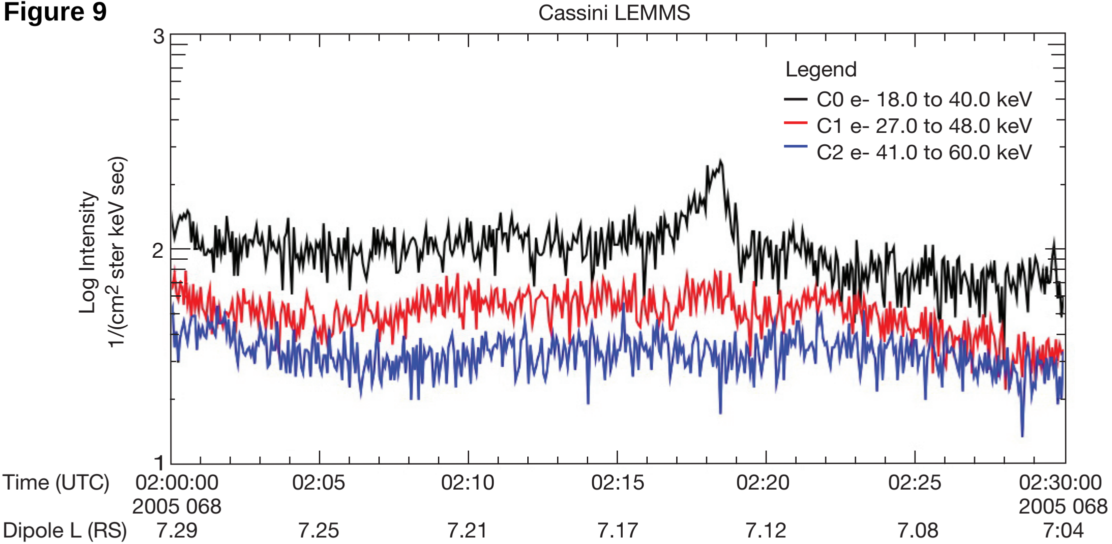
Cassini LEMMS
Legend
C0 e- 18.0 to 40.0 keV
C1 e- 27.0 to 48.0 keV
C2 e- 41.0 to 60.0 keV
Log Intensity
1/(cm^2 ster keV sec)
3
2
1
Time (UTC)
02:00:00
2005 068
02:05
02:10
02:15
02:20
02:25
02:30:00
2005 068
Dipole L (RS)
7.29
7.25
7.21
7.17
7.12
7.08
7:04

Figure 10

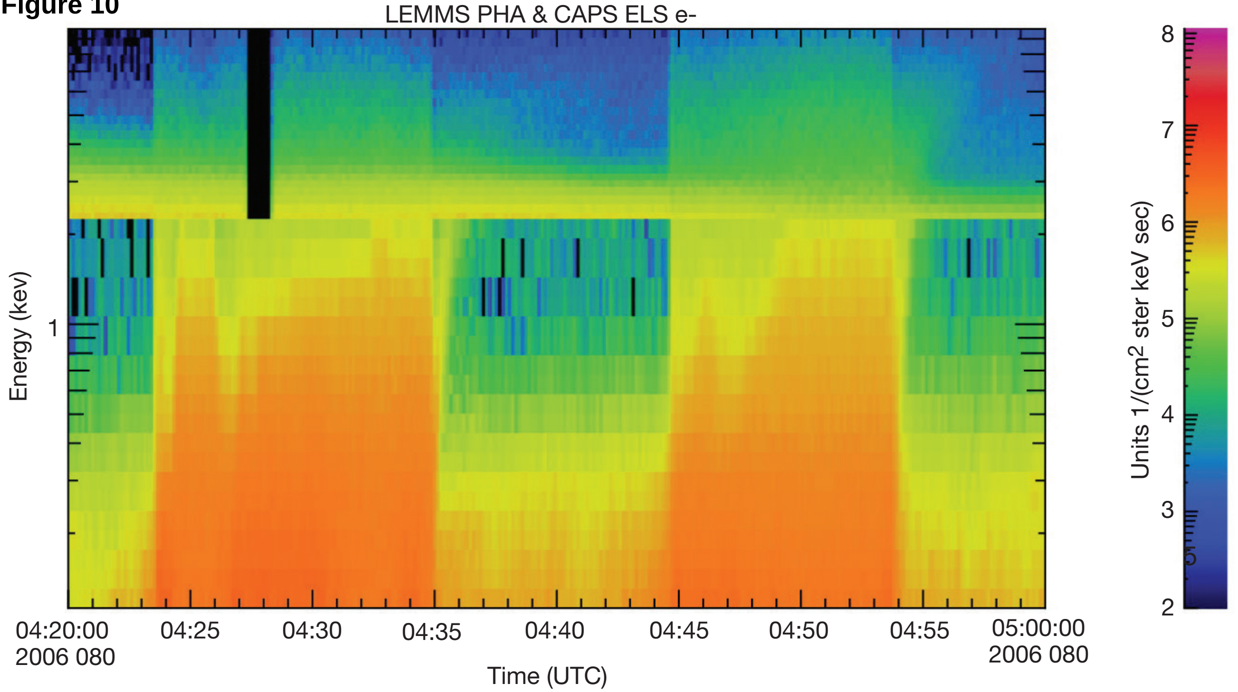
LEMMS PHA & CAPS ELS e-
Energy (kev)
1
04:20:00
2006 080
04:25
04:30
04:35
04:40
04:45
04:50
04:55
05:00:00
2006 080
Time (UTC)
Units 1/(cm^2 ster keV sec)
8
7
6
5
4
3
2

Highlights.

Method of identifying flow channel features based on recent radial transport

Inward transport of energetic charged particles limited by flow channel properties

Use data model comparisons to infer flow channel properties at Saturn